RSC Advances

This is an *Accepted Manuscript*, which has been through the Royal Society of Chemistry peer review process and has been accepted for publication.

Accepted Manuscripts are published online shortly after acceptance, before technical editing, formatting and proof reading. Using this free service, authors can make their results available to the community, in citable form, before we publish the edited article. This *Accepted Manuscript* will be replaced by the edited, formatted and paginated article as soon as this is available.

You can find more information about *Accepted Manuscripts* in the Information for Authors.

Please note that technical editing may introduce minor changes to the text and/or graphics, which may alter content. The journal's standard Terms & Conditions and the Ethical guidelines still apply. In no event shall the Royal Society of Chemistry be held responsible for any errors or omissions in this *Accepted Manuscript* or any consequences arising from the use of any information it contains.

ROYAL SOCIETY OF CHEMISTRY

www.rsc.org/advances

Journal Name

RSCPublishing

ARTICLE

Site isolation and coordination control of a transition metal ion by molecular surface engineering in mesoporous silica: case of a bio-inspired copper-polyamine grafted complex†

Cite this: DOI: 10.1039/x0xx00000x

Received 00th January 2012,
Accepted 00th January 2012

DOI: 10.1039/x0xx00000x

www.rsc.org/

Sébastien Abry, Ping Zhang,‡ Belén Albela* and Laurent Bonneviot*

A bio-inspired polyamine copper complex with an open coordination for potential applications in oxidation catalysis was homogeneously grafted in the nanopore of a mesoporous MCM41-like silica. This was achieved using a partial surface silanol capping by trimethylsilyl functions in the presence of a molecular stencil pattern (MSP) that masks the surface. This mask was then withdrawn to graft the tridentate polyamine ligand that provokes a substantial de-capping in its vicinity. Before complexation by Cu(II) ions, the surface was capped again for a better control of the hydrophobicity, which incidentally prevents not only adsorption of copper on silanol but also copper pairing for high level of MSP controlled organic coverage. Concomitantly, it appears a surprising competition of copper with its own counterion for complexation to the grafted polyamine. This effect is more pronounced for triflate ($F_3CSO_3^-$, Tf^-) than chloride (Cl^-), leading the former to be better for site isolation. The copper coordination quantitative analysis of both monomeric and dimeric species is based on a combined EPR and EXAFS investigation.

Introduction

Metalloproteins have been widely studied in biology owing to their crucial properties for oxygen transport, electron transfer and catalytic transformations. Hemocyanine, Tyrosinase and Catechol Oxydase are copper metalloproteins involved either in dioxygen storage or in dioxygen activation for oxidation processes.[1-4] They present a type-3 copper active site[5], consisting in a dicopper system in which each metal ion is chelated by three amino groups (provided by three histidines), water molecules and peroxo or oxo bridges, depending on the oxidation state of copper.[6, 7] Basically, these sites contain a copper ion in a distorted pentacoordinated environment. They have been extensively used as models to design homogeneous catalysts for oxidation.[8-10] The catalytic cycle proposed for oxidation of substrates considers two copper centers that are far apart in the reduced form, and then become closer upon activation of dioxygen, thanks to a peroxo bridge.[2, 7]

A number of studies on oxidation catalysis using these copper model complexes show that the active peroxo-copper entity can oxidize the ligand of the metallic complex prior to the substrate, leading to degradation of the catalyst.[10] Grafting the reactive metallic site on an inorganic support could inhibit this degradation process. Moreover, heterogeneous catalysis has other advantages, such as catalyst recycling, easy handling and the possibility to work in absence of solvents.

Among the different inorganic supports available, mesostructured porous silica such as MCM-41 offers the advantages of size control (homogeneous diffusion regime), high specific surface and high thermal and mechanical stability.[11-13] In particular, high specific surface allows high loading of active sites, therefore favouring the use of spectroscopic techniques such as solid NMR or IR to characterize the grafted species (see below for abbreviations). Moreover, the pore occupancy and its integrity is conveniently monitored at each step of the material preparation both using XRD patterns and nitrogen adsorption profiles.

RSC Advances Accepted Manuscript

In order to design a controlled heterogeneous catalyst a single site is required. This implies a homogeneous distribution of the tether functions that maintain the complex fixed onto the support and a control of its vicinity. Two main approaches are currently used in order to isolate functions on the surface of oxide supports such as silica: (1) high dilution of the grafted species, where the functions are statistically distributed, and (2) anchoring with molecular control in the vicinity of the grafted function using a molecular spacer or steric hindrance.[14-25] We have recently developed an alternative technique called "Molecular Stencil Patterning" (MSP) that allows control over both short and long range distances.[26-32] It consists in controlling silanol passivation using an organosilane (for example trimethylsilyl, TMS) in the presence of the templating alkylammonium ions in the mesoporous silica. The latter play the role of a molecular protecting mask, homogeneously covering the internal surface of the silica due to self-electrostatic repulsions. Indeed, the cationic ammonium heads of the surfactant molecules are attracted toward the surface by negative silanolate groups but are pushed away one from another by electrostatic repulsion leading to a homogeneous distribution of cationic surfactant molecules. After removal of the mask, the second function (a ligand for a metal ion, an acid, etc.) is grafted where the aklyammonium ion was located. The molecular stencil patterning (MSP) technique is applied here to design a bio-inspired copper heterogeneous catalyst where the amino ligand mimics the environment of the Cu active site in Catechol Oxidase and the confinement in the nano channel is meant to mimic the effect of the cavity of the enzyme. In this system, control over the natural pairing tendency of copper (II) is tuned using the MSP technique at various organic coverages and for two different metal counterions. The novel features here are the study of the counterion effect, a careful quantification of the organic coverage in various functions and a second capping treatment after the grafting of the ligand using a polyamino-organic siloxane. This brings the surface into a state of full coverage, forcing the copper ion and its own counterion to compete for complexation to polyamine, unseen in conventional solvent driven complexation.

Experimental

1. Intrumentation

XRD: low angle X-ray powder diffraction experiments were carried out using a Bruker (Siemens) D5005 diffractometer using Cu Kα monochromatic radiation. **IR**: infrared spectra were recorded from KBr pellets using a Mattson 3000 FT-IR spectrometer. **UV-Vis:** liquid UV-visible spectra were recorded using a Vector 550 Bruker spectrometer. Solid diffuse reflectance UV-visible and near infrared spectra were recorded from aluminium cells with Suprasil 300 quartz windows, using a PerkinElmer Lambda 950 and PE Winlab software. **Nitrogen sorption isotherms** at 77 K were determined with a volume device, Micromeritics ASAP 2010M. **TGA** measurements (measure of weight loss at 1273 K) were collected from Al_2O_3 crucibles on a DTA-TG Netzsch STA 409 PC/PG instrument, under air (30 mL/min), with a 298-1273K (10K/min) temperature increase. **NMR**: ^1H and ^{13}C liquid NMR spectra were recorded on a Bruker AC 200 MHz spectrometer. ^{13}C and ^{29}Si CP-MAS solid state NMR measurements were collected on a Bruker DSXv400 spectrometer (for both, cross-polarisation was used). For ^{29}Si (79.49 MHz), a 4 µs (corresponding to $\theta = \pi/3$) pulse was used with a repetition time of 4 s. For ^{13}C (100.6 MHz), a 6 µs ($\theta = \pi/2$) pulse was used with a repetition time of 3 s. The spinning rate of the rotor (7 mm diameter) was about 5 kHz and the number of scans, between 2000 and 15000, depending on the rate of grafting. For ^{29}Si MAS solid NMR, a 3.5 µs (corresponding to $\theta = \pi/4$) pulse was used with a repetition time of 60 s. The spinning rate of the rotor was about 10 kHz. **EPR** spectra were recorded using a Brucker Elexsys e500 X-band (9.4 GHz) spectrometer with a high sensibility cavity at room temperature. **XAS**: X-ray absorption spectroscopy was performed at the European Synchrotron Facility (ESRF) in Grenoble (France) on BM30 (French) and BM25 (Spanish) beam lines at the Cu K edge (8979 eV). The EXAFS signals were extracted and simulated using the EXAFS for Mac package for OSX.[33] The Fourier transformation was taken on a reasonable k range where the signal was higher than the noise, typically 2.5 to 14 $Å^{-1}$. The fit was performed using theoretical backscattering phase and amplitude functions calculated from FEFF6.[34, 35]

2. Experimental procedures and characterization

Hexadecyltrimethylammonium-*p*-toluene-sulfonate (CTATos) (>99% Merck), chlorotrimethylsilane (CTMS) (98% Acros), hexamethyldisilazane (HMDSA) (98% Acros), hexamethyldisiloxane (HMDSO)(98% Acros), Ludox HS-40 (40% SiO_2 Aldrich), (3-trimethoxysilylpropyl)diethylene triamine (DETA) (95% ABCR-Roth) and 3-bromopropyl-trichlorosilane (BPTCS) (97% ABCR-Roth) were used as received. Toluene, cyclohexane, acetonitrile were stored with molecular sieves under nitrogen.

2.1. Synthesis of as made LUS [26, 36, 37]

LUS was prepared as follows: Ludox (15.5 g, 0.26 mol) was added to sodium hydroxide (2g, $5x10^{-2}$ mol) in deionized water (50 mL), then stirred at 313 K until clear (about 24 h). A second solution of hexadecyltrimethylammonium p-toluenesulfonate (CTATos) (2.5 g, $5.5x10^{-3}$ mol) in deionized water (90 mL) was stirred for 1h at 333 K. The first solution was dropwise added to the second one, and then stirred at 333 K for 2 h. The resulting sol-gel was heated in an autoclave at 403 K for 20 h. After filtration and washing with deionized water (approximately 300mL), the as-synthesized solid was dried at 353 K. *Elemental Analysis*: C(32,7%), H(6.7%), N(2.0%), S(0.4%), *weight loss* at 1273 K (49.3%). BET specific surface area of 970 $m^2.g^{-1}$ was obtained after solvent extraction (see below) and vacuum treatment at 423 K for 4 h.

2.2. Partial extraction: LUS-Ex%, x = 25, 50, 75

RSC Advances Accepted Manuscript

5 g of as-made material LUS was solved in technical ethanol (120 mL) and stirred at 313 K for a few minutes, then diluted hydrochloric acid 1 mol.L^{-1} (standard, Acros) was added. The quantity depends on the quantity of surfactant to be removed (1.7 mL (0.25 eq), 3.4 mL (0.50 eq) and 5.1 mL (0.75 eq), leading respectively to LUS-E25%, LUS-E50% and LUS-E75%). The mixture was stirred at 313 K for 1 hour, then filtered, washed with technical ethanol (3 x 70 mL), technical acetone (2 x 50 mL), and dried at 353K for one night, leading to between 3 and 4 g of partially extracted silica.

Elemental Analysis - LUS-E25%: C(24.4%), H(5.1%), N(1.3%), *weight loss* at 1273 K (31.8%). LUS-E50%: C(22.0%), H(4.7%), N(1.0%), Si(30.5%). LUS-E75%: C(16.6 %), H(3.7 %), N(0.7%), *weight loss* at 1273 K (18.5%).

2.3. Partial silylation: Sn

3 g of partially extracted silica LUS-Ex% was placed in a round bottom two-neck flask where it was dried at 423 K under argon flow for 1 hour, then under vacuum for 2 hours. Upon return to room temperature, cyclohexane (100 mL) and hexamethyldisilazane HMDSA (20 mL) were added to the flask, then the mixture was stirred at room temperature for 1 hour, and further refluxed for 17 hours. The mixture was filtered, washed with cyclohexane (3x70 mL), technical ethanol (3x70 mL), acetone (50mL), and dried at 353K for one hour. All these steps were repeated twice followed by an overnight drying at 353 K, leading to between 2 and 3 g of partially silylated silica Sn. After silylation LUS-E25%, LUS-E50% and LUS-75% respectively gave solids S1, S2 and S3,.

Elemental Analysis - S1: C(24.2%), H(5.1%), N(1.3%), *weight loss* at 1273 K (31.8%). S2: C(22.0%), H(4.7%), N(1.0%), Si(30.5%). S3: C(16.6%), H(3.7%), N(0.7%), *weight loss* at 1273 K (18.5%).

2.4. Extraction of remaining surfactant: Sn-E

3 g of partially silylated silica Sn was solved in technical ethanol (180 mL) and stirred at room temperature. 1.1 equivalent of hydrochloric acid 1 mol.L^{-1} was added. The mixture was stirred 1 hour, then filtered, washed with technical ethanol (3x70 mL), acetone (2x50 mL), and dried at 353 K for one night, leading to between 2 and 2.5 g of extracted silica Sn-E. *Elemental Analysis* – S1-E: C(1.9%), H(1.5%), N(<0.10%), *weight loss* at 1273 K (11.0 %). S2-E: C(4.1%), H(1.6%), N(<0.10%), *weight loss* at 1273 K (8.7%). S3-E: C(5.9%), H(2.0%), N(<0.10%), *weight loss* at 1273 K (11.5 %).

2.5. Diethylenetriaminepropyl functionalization: Sn-L (L = DETA)

Sn-E (3g) was placed in a round bottom two-neck flask dried at 403 K for 1h under nitrogen flow then 2 h under vacuum. The solid was solubilized in 50 mL of toluene. 3-(trimethoxysilylpropyl)diethylenetriamine (DETA) (15 mL for S1-E, 10 mL for S2-E and 5 mL for S3-E) was added under nitrogen flow. The mixture was stirred at room temperature for 1 hour, and further refluxed for 17 hours. The obtained product was washed with toluene (3x40 mL), technical ethanol (3x40 mL) and acetone (1x30 mL). The solids were dried at 353 K, leading to between 3.2 and 3.4g of Sn-L. *Elemental Analysis* - S1-L: C(13.9%), H(3.3%), N(6.1%), Cl(1.0%), *weight loss* at 1273 K (25.7%). S2-L: C(14.0%), H(3.3%), N(5.9%), Cl(0.2%), *weight loss* at 1273 K (26.7%). S3-L: C(13.3%), H(3.2%), N(4.7%), Cl(0.4%), *weight loss* at 1273 K (21.6%).

2.7. Capping: Sn-L-C

2 g of silica Sn-L were placed in a round bottom two-neck flask, where it was dried at 353 K under argon flow for 1 hour, then under vacuum for 2 hours. Upon return to room temperature, cyclohexane (50 mL) and hexamethyldisilazane HMDSA (10 mL) were added to the flask, then the mixture was stirred at room temperature for 1 hour, and refluxed for 17 hours. The mixture was filtered, washed with cyclohexane (3x40 mL), technical ethanol (3x40 mL) and acetone (30 mL). The bifunctionalised solids were dried at 353 K overnight, leading to about 2 g of Sn-L-C.

Elemental Analysis - S1-L-C: C(15.7%), H(3.7%), N(5.6%), *weight loss* at 1273K (27.4%). S2-L-C: C(15.8%), H(3.7%), N(5.3%), *weight loss* at 1273K (25.8%). S3-L-C: C(14.3%), H(3.4%), N(4.6%), *weight loss* at 1273K (23.6%).

2.8. Complexation with copper: Sn-L-C-Cu-Cl and Sn-L-C-Cu-Tf

200 mg of bifunctional solid Sn-L-C was placed in a round bottom flask with 5mL of technical ethanol. In parallel, two solutions of $CuCl_2$ and $Cu(Tf)_2$ in ethanol were prepared at 3.4 10^{-2} mol.L^{-1}. Then 4.8 or 12 mL of the copper solution were respectively added to the solid suspension, depending on the TMS coverage (S1, S2 or S3) of the sample. The mixture was stirred at room temperature for 20 min, filtered and then washed 3 times with technical ethanol. The obtained silica were dried at room temperature for two days, leading to about 0.2 g of solid. The –Cu-Cl suffix in the name of the sample stands for metalation with copper(II) chloride and –Cu-Tf for metalation with copper(II) trifluoroacetate.

Elemental Analysis - S1-L-C-Cu-Cl: C(12.2%), H(3.4%), N(4.3%), Cl(7.0%), Cu(6.4%), *Si*(25.8%). S2-L-C-Cu-Cl: C(12.1%), H(3.8%), N(4.1%), Cl(6.0%), Cu(5.9%), *Si*(24.1%). S3-L-C-Cu-Cl: C(12.5%), H(3.3%), N(4.0%), Cl(4.2%), Cu(3.7%), *Si*(28.4%). S1-L-C-Cu-Tf: C(13.0%), H(2.4%), N(3.3%), S(2.5%), F(6.2%), Cu(3.6%), *Si*(25.4%). S2-L-C-Cu-Tf: C(12.9%), H(2.9%), N(4.0%), S(2.5%), F(6.2%), Cu(3.7%), *Si*(24.6%). S3-L-C-Cu-Tf: C(12.4%), H(2.9%), N(3.6%), S(1.9%), F(5.1%), Cu(2.8%), *Si*(27.1%).

2.9. Determination of functions loading

The silicon content was calculated either from the weight loss at 1273 K from TGA experiments or from Si analysis (wt%). For better description of the material at the molecular level, all the amounts are also given in the molecular ratio related to silicon of the silica framework. The latter is called inorganic silicon (Si_{inorg}). By contrast, the organic silicon will correspond to the grafted organosilanes, either TMS or the grafted DETA amine. In addition, TMS partial grafting is compared to a totally silylated sample obtained from a full silylation using a mixture of trimethylchlorosilane in hexamethyldisiloxane in reflux. In this sample, the TMS/Si_{inorga} molar ratio is 0.23, and it

RSC Advances Accepted Manuscript

will be considered as reference for 100 % coverage of the pore surface [26, 27].

Function loading was determined considering two hypotheses. Firstly, the amount of amine ligand incorporated was calculated starting from nitrogen analysis and supposing that there was no other nitrogen source in the solid. Secondly, quantification of TMS groups was performed by quantitative infrared spectroscopy, and more precisely the integration of the peak at 846 cm^{-1}, which corresponds to the Si-C stretching band of O-Si-$(CH_3)_3$ entities. Each spectrum was previously normalized using the peak at 459 cm^{-1} (SiO_2 bending of the silicon framework), and the? baseline was corrected (see example in Fig. S1). The extra C present in the sample can be attributed to residual EtOH present in the solid.

2.10. EPR SPECTRA

EPR spectra were recorded at room temperature (298 K) with the following parameters: frequency = 9.35 GHz, power = 6.37 mW, modulation amplitude: 1G, modulation frequency: 100 kHz. Gain was adapted for each sample in order to obtain a similar intensity in the spectrum. Quantification of isolated Cu(II) species was performed using crystals of $CuSO_4.5H_2O$ as calibration reference. A double integration of the EPR signal was done after baseline correction. The number of isolated species was related to the copper content deduced from elemental analysis. Relative error was ~ 10 %.

Results and discussion

Mesoporous LUS, a 2D hexagonal MCM41-like silica was used as inorganic support owing to its high quality of ordering, large specific area (~1000 $m^2.g^{-1}$), narrow pore size distribution and high silanol density for grafting.[36, 37] Its as-made form was treated sequentially according to the molecular stencil patterning (MSP) technique[26-28] , which comprised: i) partial template extraction using the remaining surfactant as molecular surface mask patterning, ii) trimethylsilyl (TMS) capping using hexadimethylsilazane as a silanol capping agent, hydrophobic and isolation function, iii) acidic removal of the masking agent using diluted HCl solution, iv) grafting of the diethylenetriaminepropyl-triethoxysilane to fix the DETA tridentate polyamine ligand, v) additional post capping (C) to rebuild a full silanol capping level after step iv, and v) metalation using either copper chloride or copper triflate, CuX_2 with $X^- = Cl^-$ or $Tf^- = F_3CSO_3^-$, respectively (Fig.1, top).[27, 28] As has been shown in previous studies, this patterning technique allows a homogeneous distribution of the functions in the nanoscopic channels of the porous silica with no damage to the mesoprorous structure of the solid.[28] Three levels of partial surfactant removal were obtained yielding solids denoted as **Sn**

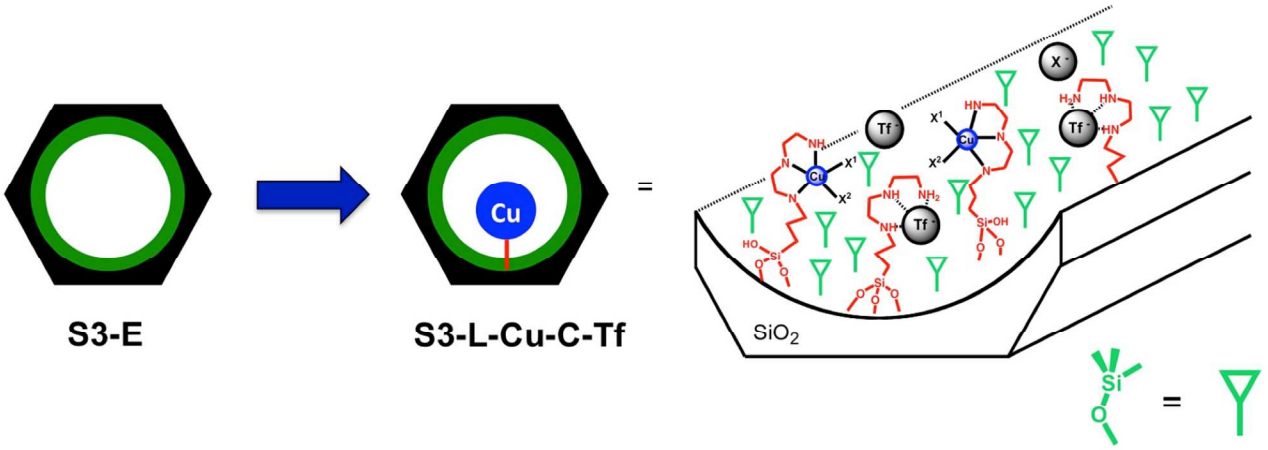

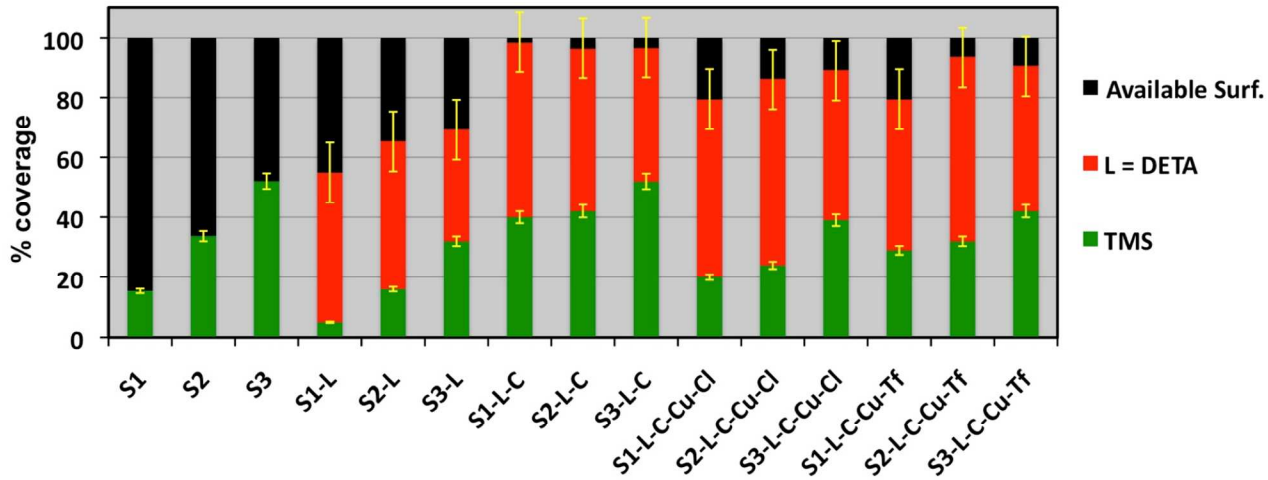

RSC Advances Accepted Manuscript

Journal Name RSCPublishing

ARTICLE

Fig. 1 Various stages of surface elaboration: (top) scheme of functionalization of LUS support to afford a typical Sn-L-C-Cu-Tf material, and (bottom) distribution of the functions on the surface of the solid, green bars for trimethylsilyl (TMS) and red bars for DETA (L); DETA determined from N elemental analyses (10% error) and TMS quantified from IR spectroscopy (5% error).

with n = 1-3 for increasing TMS loading. Then, the sequential synthesis successively produced materials **Sn**, **Sn-L**, **Sn-L-C** and **Sn-L-C-Cu-X,** which were all investigated (L = DETA and X = Cl or Tf, Fig. 1).

According to the XRD patterns, the 2D hexagonal *Pm3m* mesostructure of the functionalized silicas was maintained throughout the sequence of the organic modifications of the surface (Fig. 2A). The structure quality was notably better for an increasing level of hydrophobization, showing that a higher capping level stabilizes the structure in agreement with previous reports using different capping techniques.[38]

The nitrogen sorption isotherms of the initial mesoporous silica, **LUS**, the organically modified silicas, **Sn** and **Sn-L-C**, and the metallated solid **Sn-L-C-Cu-Cl** correspond to the type IV profile characteristic of surfactant templated mesoporous materials as exemplified for n = 3 on Fig. 2B (Table S1).[28, 39-41] Three parameters show the highest progressive decrease along the sequence: i) the total pore volume (Vp) measured by the height of the physisorption plateau taken at the relative pressure P/P_0 = 0.9, ii) the pore diameter provided by the capillary condensation position arising as a step between P/P_0 = 0.2 - 0.4, and iii) the BET constant C related to the polarity of the surface, and measured here between P/P_0 = 0.05 - 0.15 (Table S1). The pore volume reduction (0.86, 0.78, 0.49 and 0.38 ± 0.02 $mL.g^{-1}$ for **LUS**, **S3**, **S3-L-C** and **S3-L-C-Cu-Cl**, respectively) is consistent with a progressive pore filling along the sequence of functionalization. Concomitantly, the pore diameter also decreases (along the same series, 3.7, 3.4, 2.9 and 3.0 ± 0.1 nm as calculated using the Broekhoff and de Boer method, Table S1).[42, 43] This is consistent with a homogeneous distribution of functions all along the nano channels of the solid. The metalation modifies only slightly the pore size since the metal is nested in the already grafted ligand. Nonetheless, the loss of volume remains perceptible for this last step also. In addition, the BET C parameter underwent a large systematic decrease, from 105 in the genuine **LUS** down to 10 in the **S3-L-C** material (before metalation). This is reminiscent of a progressive loss of surface polarity upon higher coverage of organic functions (TMS+L, *vide infra*). By contrast, complexation by Cu(II) reversed the trend with a modest increase of C from 10 to *ca.* 31 calling into question the charge of the grafted metal complex, the presence and position of the counterion in the coordination of copper and its oxidation state.

Focusing first on analytical data, the loading of the ligand L was *ca.* 1 $mmol.g^{-1}$ according to nitrogen content regardless of the TMS initial coverage (Table S2). The titration of TMS obtained from quantitative infrared (IR) analysis evidenced a neat depletion of these groups during the grafting of L (Fig. 1 and S1, and Table S2). This effect was more pronounced at low TMS coverage. Nonetheless, the re-capping step **C** was found to be efficient with a L + TMS overall surface coverage of 97 ± 7 % for all the **Sn-L-C** samples (Fig. 1, bottom). ^{29}Si CP-MAS NMR confirmed the grafting of both trimethylsilyl and the DETA-propylsilyl groups with predominantly tricoordinated T_3 species (Fig. S2). In the final metallated solids, the TMS/L ratio was similar for S1 and S2 materials, and slightly higher for S3 (Fig. 1). Hence, any difference of copper complexation can be related to a difference in the grafted functions distribution.

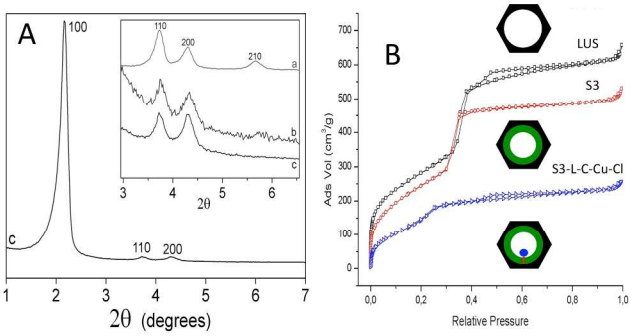

Fig. 2 (A) XRD patterns of (a) **LUS** support, (b) **S2-L-C-Cu-Cl** and (c) **S3-L-C-Cu-Cl**. (B) N_2 sorption isotherms at 77 K of the support **LUS** (□) and materials **S3** (○) and **S3-L-C-Cu-Cl** (▷). Template was extracted in all the solids.

Considering the experimental conditions used and the molecular analogues $CuLCl_2$ and $CuLTf_2$, the expected L/Cu molar ratio is 1.[44] According to elemental analyses, this is the case for **S1-L-C-Cu-Cl** and **S2-L-C-Cu-Cl** (L/Cu = 1.0 ± 0.1) but not for **S3-L-C-Cu-Cl** and for all three copper triflate materials **Sn-L-C-Cu-Tf** (L/Cu = 1.4 to 1.9, Table S3). For the latter solids, partial amine protonation already observed in similar materials[29] could be a possible explanation for the high L/Cu ratio. Since this effect is dependent on the TMS coverage and on the nature of the anion (maximum effect for **S3-L-C-Cu-Tf**), an alternative explanation is necessary. The number of ligands L effectively coordinating copper could also differ in each material, and has to be determined.

RSC Advances Accepted Manuscript

Concerning electrostatic neutrality, the expected value of X/Cu is 2 and was found systematically for the chloride series of **Sn-L-C-Cu-Cl** materials (Table S3). This was true also for the solids synthesized using $CuTf_2$, with 70 % Tf^- and 30 % Cl^- anions (Table S3). The latter anion comes from residual HCl used during the removal of CTA^+ molecules. Note that, contrary to Tf^-, Cl^- is a coordinating anion. Therefore, elucidation of the coordination of copper was investigated using various spectroscopic studies.

The blue-colored copper materials exhibited typical electronic spectra for d^9 Cu(II) ions (Fig. S3 and Table S4). The bands are systematically red-shifted by 40 nm compared to the related molecular species, which is not enough to be conclusive. Then, a systematic electron paramagnetic resonance (EPR) study was performed for the whole series of samples.

All the samples are characterized by a pseudo-axial EPR signal (g_1 = 2.23-2.25, g_2 = 2.06-2.08 and g_3 = 2.00-2.02) with a resolved hyperfine structure on the g_1 component. The apparent difference in *g* values among the samples is likely due to imperfect determination of effective g values due to different intrinsic line width. The anisotropic nature of the signal at room temperature gives evidence of intrinsic motion blockage for the copper complexes, which is characteristic of species covalently bound to the surface of the solid. The orthorhombicity factor **δ,** $(g_1-g_2)/(g_1-g_3)$, was more or less the same (0.72 ± 1) in all materials (Table S4). This value is consistent with a distorted square pyramidal symmetry around an isolated copper ion denoted as M_{3+1+1}.[29, 44] This notation stands for a pseudo-square pyramidal symmetry based on 3 N atoms from DETA moieties and a fourth atom O or Cl in the equatorial plan, and another O or Cl atom in the axial position. At this stage of the study, a N_3X_2 environment could fit with the presence of any of the following ligands: water, hydroxo or chloride ions in X positions.[44] This Cu:L 1 to 1 stoechiometry is at odds with the analytical data and necessiatates further discussion and certainly a complementary technique such as EXAFS (*vide infra*). Indeed, the EPR fingerprint of the material is restrained to the isolated Cu^{II} (S = 1/2) species (no other signal was detected at half-resonant field as expected for some putative S_T = 1 copper pairs).

Hence, a quantitative EPR study was performed on the EPR active S =1/2 systems to quantify the presence of any EPR silent antiferromagnetic copper dimers (S_T = 0) such as those often formed with hydroxo or chloride bridging ligands. Fig. 4 correlates the percentage of EPR active copper (monomer, S = 1/2) in the material with silylation level (**Sn**) and copper counterion (Cl^- *vs* Tf^-). Both **S3** solids and samples containing triflate afforded 100% of Cu monomeric species. By contrast, **S1** and **S2** prepared from the chloride salt showed only ~ 70% of Cu monomer. The missing 30% is assigned to copper dimers. So, despite very little differences of concentration and L/TMS ratio in all the **Sn-L-C-Cu-Cl** samples, the MSP afforded better conditions for site isolation in **S3** solids. This shows that the trimethylsilyl degrafting observed when the ligand L was grafted did not erase the molecular stencil patterning effect. It

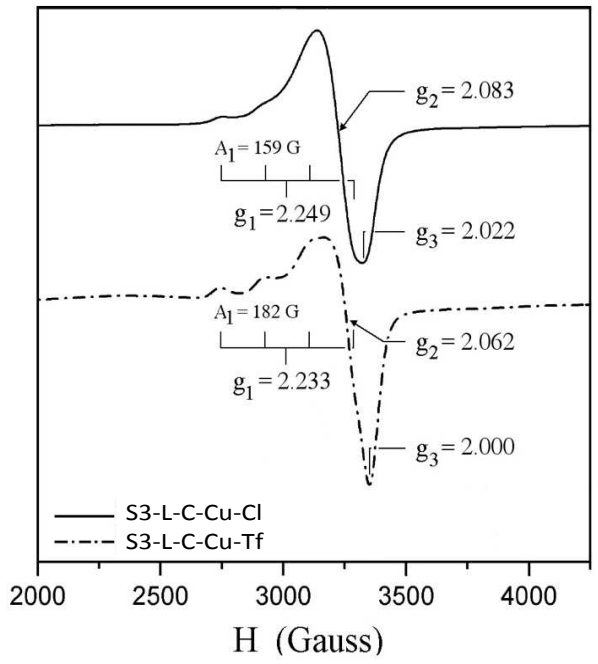

Fig. 3 X-band EPR spectra at 298 K of DETA functionalized mesostructured LUS silica after metalation by either copper chloride or copper triflate: S3-DETA-C-Cu, S3-DETA-C-Cu-Tf.

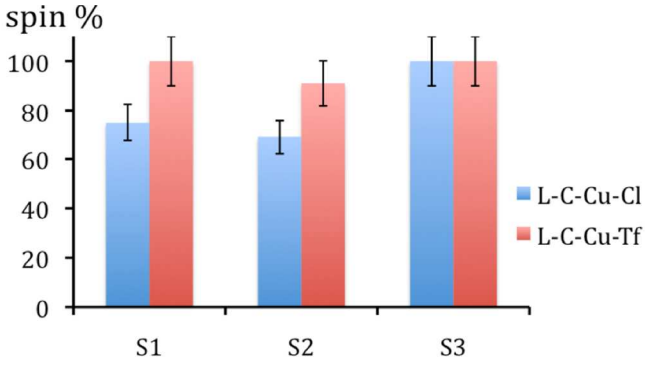

Fig. 4 Copper EPR active species (in spin %) *versus* (silylation: S1, S2 and S3) and counterion (Cl^- or Tf^-). See quantification details in the experimental part.

is worth recalling that degrafting occurs via nucleophilic substitution on the grafted silicon atom, which is catalyzed by the amino groups of L. The catalytic efficiency is certainly aided by the entropy effect when the ligand is grafted. If one assumes that self-degrafting is negligible, *i.e.,* the position of the ligand is determined by the position available at the beginning of the synthesis sequence. Then, the de-grafting action likely inhibits subsequent grafting in the vicinity of L. Hence, the "memory effect" would come from a rather rapid irreversible grafting of the polyamino ligand for a relatively slower degrafting process in the vicinity so that the masking effect has time to take place.

RSC Advances Accepted Manuscript

The last point to shed light on is the effective coordination of copper (II) ions that was investigated using EXAFS analysis on the grafted copper species and their molecular analogues. The EXAFS experimental and calculated spectra of **S3-L-C-Cu-Cl** and **S1-L-C-Cu-Cl** are compared in Fig. 5, whereas the EXAFS spectra of the molecular analogues are shown in Fig. S4, S5 and S6. The structural parameters for the molecular complexes and the materials are provided in Table S5 and Table S6, respectively. The N_3X_2 distorted square pyramidal geometry anticipated from the structure of the molecular analogues and deduced from the EPR analysis was imposed in order to decrease the number of variable parameters for the EXAFS simulation of the grafted species.[44] Thus, the coordination number was fixed at 5 with three equivalent N and two non-equivalent O or Cl atoms. In addition, four C second neighbors were taken into account and a Cu-Cu contribution was considered with a percentage provided by the quantitative EPR study (*vide supra*). The study of the molecular analogues shows

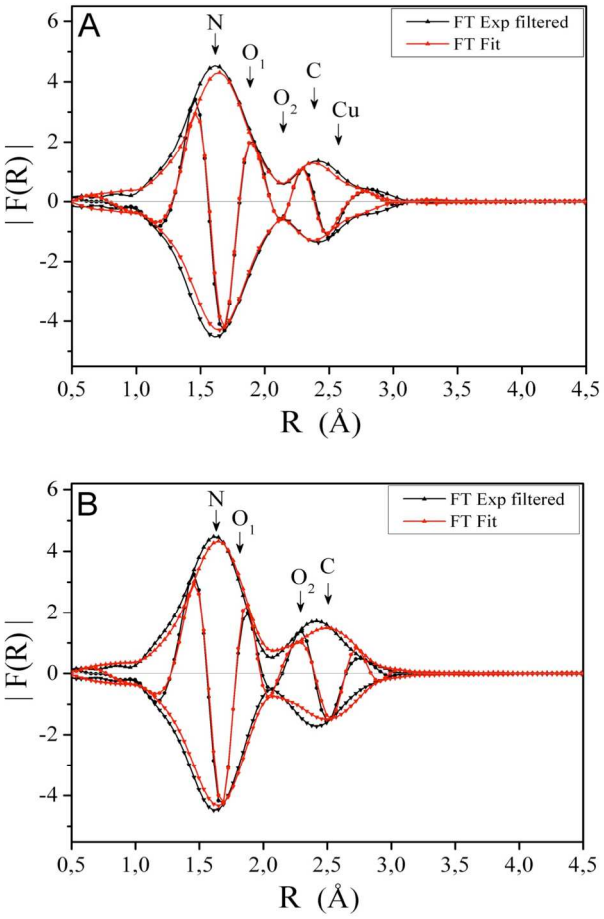

Fig. 5 Cu k edge EXAFS experimental and calculated spectra of **(A)** S3-L-C-Cu-Cl and **(B)** S1-L-C-Cu-Cl.

that i) a good fit requires considering all the first and second neighbors including C, as well as, potentially, the Cu absorbers, ii) O and Cl atoms can be distinguished in the first coordination sphere, and iii) the simulation allows to obtain distances very close to those of the model. The only variables were distances and Debye-Waller factors. The quality of the simulation was estimated from the QF parameter, which should be smaller than 1 (Table S5).

The Fourier transform (FT) of both molecular and grafted species exhibits mainly two peaks between 1 and 3.5 Å, where the distances are not phase-corrected and appear smaller than the real ones. The first peak, centered at *ca.* 1.6 Å, corresponds mainly to Cu-N contributions. The second peak, centered at 2.4 Å, arises where the carbon second neighbors are expected. The two X^n (X = O or Cl, n = 1,2) contributions in the first coordination sphere of Cu arise in between these two peaks. Indeed, they generate a negative interference, lowering the intensity of both first and second FT peaks (Fig. 5). This is why the simulation has to be performed with all the shells simultaneously. Finally, the Cu-Cu contribution appears around 2.6 Å also as a negative interference decreasing the second peak intensity. The simulation shows that there is no Cl in the coordination sphere of Cu in all the grafted species. The Cu-N, Cu-O^1 and Cu-O^2 distances for **S3-L-C-Cu-Cl** are 202 ± 1, 213 ± 3 and 241 ± 4 pm, respectively (Fig. 5 and Table S6). A single water ligand may appear in apical position at 220-240 pm for copper complexes with aminoligands. [45, 46, 47]Cu-O_{water} distances for water molecules in the axial position can be even higher, such as 263 pm in the *trans*-bis[2,3-diamino-*(R,S)*-propionato-*N,N'*]diaquacopper(II) complex reported by Champan *et al.*[48] However, when water is in the equatorial position, Cu-O_{water} distances of about 200 pm can be observed due to Jahn-Teller effect.[49] By comparison, the hydroxo ligand arises at much shorter distances (192-195 pm) even in □-OH bridged complexes, where also a longer distance may appear at 224 pm only in distorted double bridges.[45, 50] Therefore, the distance at 213 pm in **S3-L-C-Cu-Cl** is attributed to OH_2 in pseudo equatorial position, while the longer distance at 241 pm fits well with OH_2 in apical position.

For **S1-L-C-Cu-Cl**, that contains Cu monomers and pairs, the fit of the first shell is very similar, except that there is a lower precision in the Cu-O^1 distance and a much longer Cu-O^2 distance (250 ± 4 pm). In addition, there is a Cu-Cu distance at 310 ± 8 pm (Table S6). The lower accuracy in Cu-O^1 distance indicates that there is likely a mixture of species with different distances than those of the monomers described in **S3-L-C-Cu-Cl**. The apparent lengthening of the Cu-O^2 distance associated to a higher Debye-Waller factor (σ^2 = 120 instead of 57 pm^2) is also an indication that an additional shell of neighbors with a distance longer than the Cu-O^2 has to be considered. A very similar effect is observed for **S2-L-C-Cu-Cl** that also contains EPR silent copper pairs (32%, as compared with 35% for the former). Double hydroxo (like oxo) bridges generate Cu-Cu distances in the range 284-289 pm that are too short to fit the 310 pm found here. A mixed (μ–OH)(μ–H_2O) double bridge would fit better with the reported Cu-Cu distances of *ca.* 304 pm for a N_3X_2 environment. The quasi-perfect stoichiometry of 2 Cl^- and 1 grafted DETA per copper suggests that there are no hydroxo groups in the coordination sphere of copper.

RSC Advances Accepted Manuscript

Therefore, a double μ–H_2O bridge is more likely the appropriate solution for the dimer structure. Note that stable metal dimers with water as a bridging ligand are rare and imply, as far as we know, two other bridging ligands, such as either two guanazole ligands or a hydroxo and an acetato ligand.[45, 51, 52] It is clear that randomly grafted DETA ligands would present an environment that favors such dimer formation, which cannot be fully avoided in **S1-L-C-Cu-Cl** and **S2-L-C-Cu-Cl**. By contrast, a sufficiently high TMS coverage deposited prior to the DETA grafting in **S3-L-C-Cu-Cl** eliminates such an eventuality by imposing larger distances between the ligands.

These results suggest that the dimer species are of the D_{2+1+2} type, with 2 N from the DETA amine in the equatorial plane and 1N in the axial one, the two O from the water bridges being also in the equatorial position (Fig. S7).

The last striking point is the high L/Cu molar ratio deduced from the chemical analyses for some of the materials (up to 1.9), which is not in agreement with the L/Cu value of 1 deduced from the EPR study in full consistency with the EXAFS data. Therefore, this ratio is reminiscent of the blockage or the occupancy of the grafted DETA ligand to another action that complexing copper(II) ions. This has to be a strong effect since copper is known to be one of the strongest complexing ions among divalent transition metal ions. Note that this effect appears for the highest MSP coverage and for the triflate counterion, while none of them participate directly in the coordination sphere of copper. In addition, it is worth noting that Cl^- is much smaller and better solvated in polar solvents than Tf^- ions. Therefore, the former presents higher affinity for the polar silica surface, while the second will exhibit a higher affinity for the less polar grafted organic functions. Since, both the divalent copper ion and its two monovalent anions have to enter into the nanochannel in close vicinity, some of the polyamino groups are "requisitioned" by the anions to minimize their energy to compensate for the poor solvation capacity of the hydrophobized silica innerchannels. This is reasonable, since polyamines are effectively known to precipitate in various states of protonation, leading to a propensity for chelating interactions with anions such as triflate, nitrate or perchlorate.[53] The peculiarity here is that it occurs in the presence of copper(II), usually a deadly competitor against oxoanions in conventional analytical conditions. This effect also takes place to a lesser extent with chloride, which has a higher capacity than triflate anions to come closer to the silica polar surface for greater stabilization.

Conclusions

Bio-inspired copper complexes grafted on mesoporous LUS silica were synthesized using a molecular stencil patterning approach with diethylenetriamine (DETA) as a model ligand. The ligands are distributed on the internal pore surface by using trimethylsilyl hydrophobic functions (TMS) as spacers. This technique allows the incorporation of a high amount of isolated copper complexes (~ 1 $mmol.g^{-1}$) in the solid.

The molecular stencil pattering approach using hydrophobic TMS spacers is a technique that directly controls site isolation at relatively high metal loading and high ligand complexation efficiency. In complement, the choice of the counterion can further improve site isolation by introducing a competition for complextion by the ligand to the detriment of the metal loading. This is the case of triflate in comparison to chloride. Monitoring the coordination of copper using mainly quantitative EPR and EXAFS spectroscopies showed these competitive phenomena. In a more TMS silylated sample with isolated sites, both chloride and triflate ions generate isolated monomeric species. However, when the silylation is not enough, copper dimers likely bridged by two μ–OH_2 can be formed together with the monomeric species in the case of chloride, whereas only isolated species are observed in the case of triflate. Indeed, the more hydrophobic triflate ion has to be stabilized by the amino ligand in absence of available silanol groups, which generates an anion-cation competition for the ligand. Therefore, in the case of using $CuTf_2$ compared to $CuCl_2$, metal sites are more isolated to the detriment of a lower metal complexation of the grafted ligand.

This synthetic strategy, where surface engineering controls both site isolation and metal coordination can be extended to develop new heterogeneous catalysts with well-defined isolated sites. Mesoporous silica is known to be a thermally stable material with a porous structure that can be maintained up to 800°C under dry conditions and in boiling water for some hours.[54-56] The materials here studied can be easily dried at 80 °C overnight. For more drastic treatment the ligand is oxidised and the complexes destroyed. Nonetheless, such systems are meant to be used as catalysts in soft conditions, for example, in solvents such as water, ethanol or acetonitrile and below 100°C.

Acknowledgements

This work was supported by the "Région Rhône-Alpes", which financed both the equipment and post-doctoral internship of P. Zhang. XAS measurements were recorded at the European Synchrotron Facility (ESRF) in Grenoble (France) on BM30 (French) and BM25 (Spanish) beam lines. We thank the researchers involved in these lines for their help during EXAFS measurements.

Abbreviations

DETA, diethylenetriamine; DR UV, diffuse reflectance ultra-violet; EPR, electron paramagnetic resonance; EXAFS, extended X-Ray absorption fine structure; IR, infra-red; LUS, Laval University silica; MSP, molecular stencil pattering; NMR, nuclear magnetic resonance; Tf, trifluoromethanesufonate (triflate); TMS, trimethylsilyl; XRD: X-ray diffraction.

Notes and references

RSC Advances Accepted Manuscript

Laboratoire de Chimie, UMR 5182 CNRS, Ecole Normale Supérieure de Lyon, Université de Lyon, 46 Allée d'Italie, 69364 Lyon Cedex-07, France . Fax: +33-472728860; Tel: +33-472728856. E-mail: belen.albela@ens-lyon.fr.
‡Present address of P. Zhang: Key Laboratory of Inorganic Synthesis Preparative Chemistry, Department of Chemistry, Jilin University, Changchun 130023, China.

† Electronic Supplementary Information (ESI) available: detailed experimental procedures and characterization by chemical analyses, IR, solid ^{29}Si-NMR, DR UV-visible and EXAFS spectroscopies. See DOI: 10.1039/b000000x/

1. C. Eicken, B. Krebs and J. C. Sacchettini, *Curr. Opin. Struct. Biol.*, 1999, **9**, 677-683.
2. C. Gerdemann, C. Eicken and B. Krebs, *Acc. Chem. Res.*, 2002, **35**, 183-191.
3. S. J. Lippard and J. M. Berg, *Principles of Bioinorganic Chemistry*, University Science Books, Mill Valley, CA, 1994.
4. A. Volbeda and W. G. J. Hol, *J. Mol. Biol.*, 1989, **209**, 249-279.
5. I. A. Koval, P. Gamez, C. Belle, K. Selmeczi and J. Reedijk, *Chem. Soc. Rev.*, 2006, **35**, 814-840.
6. E. I. Solomon, M. J. Baldwin and M. D. Lowery, *Chem. Rev.*, 1992, **92**, 521-542.
7. E. I. Solomon, U. M. Sundaram and T. E. Machonkin, *Chem. Rev.*, 1996, **96**, 2563-2605.
8. E. A. Lewis and W. B. Tolman, *Chem. Rev.*, 2004, **104**, 1047-1076.
9. L. M. Mirica, X. Ottenwaelder and T. D. P. Stack, *Chem. Rev.*, 2004, **104**, 1013-1045.
10. L. Que and W. B. Tolman, *Angew. Chem. Int. Ed.*, 2002, **41**, 1114-1137.
11. A. Corma, *Chem. Rev.*, 1997, **97**, 2373-2419.
12. F. Hoffmann, M. Cornelius, J. Morell and M. Froba, *Angew. Chem. Int. Ed.*, 2006, **45**, 3216-3251.
13. K. Moller and T. Bein, *Chem. Mater.*, 1998, **10**, 2950-2963.
14. K. O. Hwang, Y. Yakura, F. S. Ohuchi and T. Sasaki, *Mater. Sci. Eng., C*, 1995, **3**, 137-141.
15. C. W. Jones and M. W. McKittrick, *Abstr. Pap. Am. Chem. Soc.*, 2003, **225**, U83-U83.
16. A. Katz and M. E. Davis, *Nature*, 2000, **403**, 286-289.
17. M. W. McKittrick and C. W. Jones, *Chem. Mater.*, 2003, **15**, 1132-1139.
18. Y. S. Shin, J. Liu, L. Q. Wang, Z. M. Nie, W. D. Samuels, G. E. Fryxell and G. J. Exarhos, *Angew. Chem. Int. Ed.*, 2000, **39**, 2702-2707.
19. D. C. Tahmassebi and T. Sasaki, *J. Org. Chem.*, 1994, **59**, 679-681.
20. G. Wulff, B. Heide and G. Helfmeier, *J. Am. Chem. Soc.*, 1986, **108**, 1089-1091.
21. G. Wulff, B. Heide and G. Helfmeier, *React. Polym.*, 1987, **6**, 299-310.
22. M. W. McKittrick and C. W. Jones, *J. Catal.*, 2004, **227**, 186-201.
23. J. C. Hicks, R. Dabestani, A. C. Buchanan and C. W. Jones, *Chem. Mater.*, 2006, **18**, 5022-5032.
24. D. Bruehwiler, *Nanoscale*, 2010, **2**, 887-892.
25. K. K. Sharma, R. P. Buckley and T. Asefa, *Langmuir*, 2008, **24**, 14306-14320.
26. S. Abry, B. Albela and L. Bonneviot, *C. R. Chim.*, 2005, **8**, 741-752.
27. A. Badiei, L. Bonneviot, N. Crowther and G. M. Ziarani, *J. Organomet. Chem.*, 2006, **691**, 5911-5919.
28. S. Abry, F. Lux, B. Albela, A. Artigas-Miquel, S. Nicolas, B. Jarry, P. Perriat, G. Lemercier and L. Bonneviot, *Chem. Mater.*, 2009, **21**, 2349-2359.
29. S. Abry, A. Thibon, B. Albela, P. Delichère, F. Banse and L. Bonneviot, *New J. Chem.*, 2009, **33**, 484-496.
30. K. Zhang, B. Albela, M. Y. He, Y. M. Wang and L. Bonneviot, *PCCP*, 2009, **11**, 2912-2921.
31. W. J. Zhou, B. Albela, M. G. Ou, P. Perriat, M. Y. He and L. Bonneviot, *J. Mater. Chem.*, 2009, **19**, 7308-7321.
32. V. Jollet, B. Albela, K. Senechal-David, P. Jegou, E. Kolodziej, J. Sainton, L. Bonneviot and F. Banse, *Dalton Trans.*, 2013, **42**, 11607-11613.
33. A. Michalowicz, *EXAFS pour le Mac*, (1991) Societé Française de Chimie, Paris.
34. J. J. Rehr, J. M. Deleon, S. I. Zabinsky and R. C. Albers, *J. Am. Chem. Soc.*, 1991, **113**, 5135-5140.
35. J. J. Rehr, R. C. Albers and S. I. Zabinsky, *Phys. Rev. Lett.*, 1992, **69**, 3397-3400.
36. L. Bonneviot, M. Morin and A. Badiei, 2001, vol. WO 01/55 031A1.
37. P. Reinert, B. Garcia, C. Morin, A. Badiei, P. Perriat, O. Tillement and L. Bonneviot, in *Nanotechnology in Mesostructured Materials*, Elsevier Science Bv, Amsterdam, 2003, vol. 146, pp. 133-136.
38. T. Tatsumi, K. A. Koyano and N. Igarashi, *Chem. Commun.*, 1998, 325-326.
39. J. S. Beck, J. C. Vartuli, W. J. Roth, M. E. Leonowicz, C. T. Kresge, K. D. Schmitt, C. T. W. Chu, D. H. Olson, E. W. Sheppard, S. B. McCullen, J. B. Higgins and J. L. Schlenker, *J. Am. Chem. Soc.*, 1992, **114**, 10834-10843.
40. C. T. Kresge, J. C. Vartuli, W. J. Roth and M. E. Leonowicz, in *Mesoporous Crystals and Related Nano-Structured Materials*, 2004, vol. 148, pp. 53-72.
41. C. T. Kresge, J. C. Vartuli, W. J. Roth, M. E. Leonowicz, J. S. Beck, K. D. Schmitt, C. T. W. Chu, D. H. Olson, E. W. Sheppard, S. B. McCullen, J. B. Higgins and J. L. Schlenker, in *Science and Technology in Catalysis 1994*, 1995, vol. 92, pp. 11-19.
42. Note that the BdB method lead to pore size values close within 0.1 nm to those obtained from DFT and both techniques are more reliable methods than commonly used BJH, which provides a values 0.7 nm smaller, i. e., 3.0-3.2 nm often reported for MCM-41 templated by cetyltrimethylbromide, CTAB. For smaller values the difference increases, for instance 2.2 nm (BJH) for 3.0 nm (BdB).
43. J. C. P. Broekhoff and J. H. De Boer, *J. Catal.*, 1968, **10**, 153-165.
44. M. J. Bew, B. J. Hathaway and R. J. Fereday, *J. Chem. Soc., Dalton*, 1972, 1229-1237.
45. I. Chadjistamatis, A. Terzis, C. P. Raptopoulou and S. P. Perlepes, *Inorg. Chem. Commun.*, 2003, **6**, 1365-1371.
46. H. C. Freeman, M. R. Snow, I. Nitta and K. Tomita, *Acta Crystallographica*, 1964, **17**, 1463-1470.

RSC Advances Accepted Manuscript

47. B. M. Casari, A. H. Mahmoudkhani and V. Langer, *Acta Crystallogr., Sect. E: Struct. Rep. Online*, 2004, **60**, m1949-m1951.
48. J. Chapman, N. L. Pickett, G. Kolawole, M. Motevalli and P. O'Brien, *Acta Crystallogr., Sect. C: Cryst. Struct. Commun.*, 2000, **56**, e501-e502.
49. P. Frank, M. Benfatto, R. K. Szilagyi, P. D'Angelo, S. D. Longa and K. O. Hodgson, *Inorg. Chem.*, 2005, **44**, 1922-1933.
50. M. J. Belousoff, M. B. Duriska, B. Graham, S. R. Batten, B. Moubaraki, K. S. Murray and L. Spiccia, *Inorg. Chem.*, 2006, **45**, 3746-3755.
51. G. Christou, S. P. Perlepes, E. Libby, K. Folting, J. C. Huffman, R. J. Webb and D. N. Hendrickson, *Inorg. Chem.*, 1990, **29**, 3657-3666.
52. E. Aznar, S. Ferrer, J. Borras, F. Lloret, M. Liu-Gonzalez, H. Rodriguez-Prieto and S. Garcia-Granda, *Eur. J. Inorg. Chem.*, 2006, 5115-5125.
53. P. C. Junk, Y. Kim, B. W. Skelton and A. H. White, *Z. Anorg. Allg. Chem.*, 2006, **632**, 1340-1350.
54. Z. A. AlOthman and A. W. Apblett, *Appl. Surf. Sci.*, 2010, **256**, 3573-3580.
55. J. M. Kisler, M. L. Gee, G. W. Stevens and A. J. O'Connor, *Chem. Mater.*, 2003, **15**, 619-624.
56. K. Cassiers, T. Linssen, M. Mathieu, M. Benjelloun, K. Schrijnemakers, P. Van Der Voort, P. Cool and E. F. Vansant, *Chem. Mater.*, 2002, **14**, 2317-2324.

RSC Advances Accepted Manuscript